Analytical and Bioanalytical Chemistry
https://doi.org/10.1007/s00216-019-02240-z

RESEARCH PAPER

Construction of electrochemical sensing interface towards Cd(II) based on activated g-C_3N_4 nanosheets: considering the effects of exfoliation and protonation treatment

Yao Liu [1] · Ge-Ling Wen [1,2] · Xing Chen [1,3,4] · Rohan Weerasooriya [1,5] · Zhan-Yong Hong [1] · Lian-Chao Wang [4] · Zhong-Jia Huang [2] · Yu-Cheng Wu [1,3]

Received: 30 September 2019 / Revised: 20 October 2019 / Accepted: 24 October 2019

Abstract

There is an urgent need to construct highly selective low-cost sensors for fast detection of toxic metal ions such as cadmium. When compared with 3D bulk materials, 2D layered materials after activation treatments show superior performances for electrochemical metal ion detection. The bulk graphitic carbon nitride (hereafter b-g-C_3N_4) was prepared by thermal polymerization with urea as a precursor; it was then activated through ultrasonic liquid exfoliation and protonation which resulted in successful fabrication of activated ultrathin g-C_3N_4 nanosheets (hereafter a-g-C_3N_4). The a-g-C_3N_4-modified glassy carbon electrode demonstrates excellent electrochemical performances for Cd^{2+} detection with 22.668 μA/μM sensitivity and 3.9 nM LOD (S/N = 3) due to high specific surface area and active sites created on the 2D layered structure. The chemical interference of Pb^{2+}, Cu^{2+}, and Hg^{2+} on Cd^{2+} detection was minimal. We have also measured Cd^{2+} in natural water and rice samples using the newly developed a-g-C_3N_4-modified electrode with high spike recoveries. Our results demonstrate the potential applications of newly developed a-g-C_3N_4-modified electrode for rapid detection of toxic metal ions in different sample matrixes.

Keywords Cadmium ions · Activated g-C_3N_4 nanosheets · Electrochemical detection · Exfoliation · Protonation

Introduction

Environmental pollution by heavy metal ions (HMIs) is one of a pressing problem facing the world today. Even at very low concentrations, the HMI exerts a significant damage to humans and ecological systems [1, 2]. The high proportion of human exposure to cadmium is received from the food. Therefore, cadmium in food is listed as a priority pollutant by WHO. Metallothionein is a protective protein against low levels of exposure to Cd^{2+} in humans. If the amount of cadmium bio-absorbed exceeds the complexation capacity of metallothionein, the free Cd^{2+} tends to accumulate mainly in the kidney and liver in the human body. Further, due to comparable ion radius ratios, Ca^{2+} can exchange for Cd^{2+} in bones and

Electronic supplementary material The online version of this article (https://doi.org/10.1007/s00216-019-02240-z) contains supplementary material, which is available to authorized users.

✉ Xing Chen
xingchen@hfut.edu.cn

✉ Lian-Chao Wang
hfutwlc@163.com

✉ Zhong-Jia Huang
hzj@ahpu.edu.cn

1 Key Lab of Aerospace Structural Parts Forming Technology and Equipment of Anhui Province, Institute of Industry and Equipment Technology, Hefei University of Technology, Hefei 230009, Anhui, China

2 School of Mechanical and Automotive Engineering, Anhui Polytechnic University, Wuhu 241000, Anhui, China

3 School of Resources and Environmental Engineering, Hefei University of Technology, Hefei 230009, Anhui, China

4 School of Materials Science and Engineering, Hefei University of Technology, Hefei 230009, Anhui, China

5 National Institute of Fundamental Studies, Kandy 20000, Sri Lanka

Published online: 27 November 2019

they become porous which results them to fracture and collapse, i.e., *itai-itai* disease [3, 4]. Furthermore, rice, one of the staple foods in Asia, has the highest accumulation of cadmium [5]. Therefore, development of a rapid and robust determination method for Cd^{2+} in food and water is listed as a priority.

To date, many reliable analytical methods such as atomic absorption spectrometry (AAS), atomic fluorescence spectrometry (AFS), and inductively coupled plasma mass spectrometry (ICP-MS) are available for the detection of Cd^{2+}. These methods require costly equipment, laborious sample preparations, and skilled operations that limit their routine applications in environmental monitoring [6]. Further, none of these methods has provision for in situ metal species analysis. In this context, methods based on electrochemistry are economical and fast, and they are capable of analyzing chemical species of metal ions in situ. The electrochemical methods are sensitive, and they do not require skilled labor. When compared to other voltammetry methods, anode stripping based on square wave applications offers extreme sensitivity, selectivity, and fast response for metal ions detection [7, 8]. However, the sensitivity and anti-interference properties of the electrochemical sensing interfaces need to be improved for their wide applications.

More recently, Lin et al. [9] studied the mutual interference between Cd^{2+} and Cu^{2+} on the GCE based on the detailed theoretical and experimental results. They noted rapid deposition of Cu^{2+} over Cd^{2+} on the electrode surface during pre-enrichment phase due to minimal kinetic hindrance. The modification of the electrode to enhance selectivity for the analyte is a viable option to overcome the interfering issues. In the past decades, nanomaterials such as graphene/CeO_2 [10] and N, S co-doped porous carbon [11] were employed in the electrochemical detection of Cd^{2+} due to its unique physicochemical properties. Some reports also show that the performance of electrochemical detection of heavy metal ions is dependent on their adsorption capacity [12–14].

Graphitic carbon nitride (hereafter g-C_3N_4) with a stacked 2D structure offers several advantages, including excellent chemical and thermal stabilities and being environmentally benign. Therefore, they are widely applied in removal and detection of pollutants [15–19]. Cai et al. [16] noted g-C_3N_4 nanosheets as a promising adsorbent with strong affinity for Cd^{2+} due to its large surface area with surface sites containing nitrogen functional groups. Shen et al. [17] prepared g-C_3N_4 by salt melt method with excellent capacity for Cd^{2+} (1.00 mmol/g), Pb^{2+} (1.36 mmol/g), Ni^{2+} (0.64 mmol/g), and Cu^{2+} (2.09 mmol/g) adsorption. And also, Wang et al. [19] fabricated electrochemical sensor for sensitive detection of Cd^{2+}. The ultrathin g-C_3N_4 nanosheets were synthesized via a thermal polymerization using melamine as raw materials and deionized water and acetic acid as bubble templates.

Generally, the layer-stacked materials need to be activated as changing the internal physical/chemical properties through exfoliation and functionalization treatment [20–22]. Wang et al. [23] prepared exfoliated nano-zirconium phosphate by liquid stripping, which has selectivity for Pb^{2+}. Compared to layered α-ZrP, the electrochemical response of exfoliated ZrP has significantly improved due to its enhanced reactivity. Hatamie et al. [18] prepared ultrathin g-C_3N_4 nanosheets with a thickness of 6 Å through liquid exfoliation by sonication. The total surface area of ultrathin g-C_3N_4 nanosheet-modified electrode was 20 times larger than bare GCE. The improved sensitivity of ultrathin g-C_3N_4 nanosheet-modified electrode for Pb^{2+} is attributed to enhanced surface area. Zhang et al. [22] activated the carbon nitride solids by HCl-mediated protonation. The protonation step enhanced substrate dispersion by creating new surface area and it also facilitates ion mobility. Both these modifications are used to improve sensing performance of g-C_3N_4 nanomaterials in electrochemical applications.

Herein, we synthesized the activated g-C_3N_4 nanosheets (hereafter a-g-C_3N_4) by exfoliation and protonation to construct electrochemical interface for the determination of Cd^{2+}. Firstly, the bulk g-C_3N_4 (hereafter b-g-C_3N_4) was prepared by thermal polycondensation with urea as a precursor. Then, the b-g-C_3N_4 was treated with liquid exfoliation by ultrasonication and then acidified with HCl. The newly prepared a-g-C_3N_4 was used to modify the glassy carbon electrode for Cd^{2+} detection with a three-electrode system. The a-g-C_3N_4 showed superior sensitivity to Cd^{2+} compared to b-g-C_3N_4 or bare GCE. The improved a-g-C_3N_4 by liquid exfoliation and protonation were characterized with SEM, XPS. The optimized a-g-C_3N_4-modified GCE sensor was used to determine Cd^{2+} in rice and natural water samples with success.

Experimental and methods

Reagents and instruments

Urea (CH_4N_2O), hydrochloric acid (HCl), and cadmium chloride ($CdCl_2$) were purchased from Sinopharm Chemical Reagent Co. Ltd. (China). Aluminum oxide powder with different sizes (Al_2O_3) was obtained from ChenHua Instruments Co., Shanghai, China. All chemicals were used as received without further purification. The ultrapure water at 18.2 MΩ was obtained from the NANOpure® Diamond™ UV water system and used to prepare all solutions.

A conventional three-electrode system—working electrode, a bare or modified glassy carbon electrode; reference electrode, Ag/AgCl; and counter electrode, Pt—was used in all electrochemical measurements using square wave anode stripping method with a high-precision potentiostat (CHI 660D ChenHua Instr., China). The surface morphologies of active substrates were characterized by a field emission scanning electron microscope (FESEM, Quanta 200 FEG, FEI

Company, USA) and high-resolution transmission electron microscopy (HRTEM, JEM-2100F, Japan). The X-ray diffraction (XRD) measurements were recorded with Cu Kα irradiation (λ = 0.15406 nm) (X'Pert PRO MPD). Near-surface elemental analyses were performed by X-ray photon spectroscopy (PHI 5000 Versa Probe, USA). The FT-IR spectra were collected by a Fourier infrared spectrometer (Nicolet 67, USA).

Synthesis of a-g-C_3N_4

The b-g-C_3N_4 was synthesized by using urea as a starting material. Briefly, 6 g urea powder was put in a semi-closed crucible and transferred it to a muffle furnace programmed at 550 °C with a ramp rate of 2 °C/min under the nitrogen atmosphere. The samples were kept at the final temperature for 4 h and then cooled. The calcined sample was powdered in a mortar to obtain a yellow b-g-C_3N_4 sample.

To synthesize exfoliated g-C_3N_4, 0.3 g powdered b-g-C_3N_4 was placed in a 500-mL glass bottle with a cap, and 300 mL isopropanol was added to prepare a 3-mg/L mixed solution. The mixture was ultrasonicated for 15 h, and the suspension was centrifuged at 3000 rpm to remove unexfoliated b-g-C_3N_4 to ensure uniformly dispersed g-C_3N_4 solution. The solution was freeze-dried to yield exfoliated g-C_3N_4 powder.

The protonation of g-C_3N_4 was similar as discussed elsewhere [22]. Typically, a 0.05 g of exfoliated g-C_3N_4 powder was placed in a 100-mL glass bottle, and 50 mL 10 M HCl solution was added to prepare a 1-mg/mL mixed solution. A uniformly mixed solution after sonicated for 2 h was centrifuged to remove supernatant. After washing three times with deionized water, the precipitate was re-dispersed in distilled water. The dispersion was freeze-dried to yield a-g-C_3N_4.

Preparation of modified electrodes

To fabricate a modified electrode, the surface of glassy carbon electrode (GCE) was polished with 1.0 μm, 0.3 μm, and 0.05 μm alumina slurries to remove any impurities. For the GCE, a successive ultrasound was applied in 1:1 HNO_3, ethanol, and deionized water for 2 min. The bare glassy carbon electrode was dried in air. The 3-mg a-g-C_3N_4 powder was dispersed in 3 mL of ultrapure water and sonicated for 30 min to yield a homogeneous suspension. The modified electrode was prepared by a simple casting method. In brief, 5 μL of a-g-C_3N_4 suspension was spread onto the surface of the cleaned GCE and left it dry at room temperature. For comparison, the b-g-C_3N_4-modified glassy carbon electrode was also prepared by the same procedure.

Rice sample collection

The digestion of rice sample was conducted according to the methods shown elsewhere [24]. The rice samples were obtained from the supermarket in Heilongjiang Province, China. One-gram rice sample and 10 mL HNO_3 were sealed and the container was placed in a pre-programed microwave digester. The digested solution is heated to remove the acid. The sample was diluted with deionized water to a final volume of 5 mL and preserved for Cd^{2+} analysis.

Electrochemical detection of Cd^{2+}

Electrochemical detection of Cd^{2+} on a-g-C_3N_4/GCE was carried out in 0.1 M NaAc-HAc (pH 5.0) by square wave anode stripping voltammetry (SWASV) under the deposition potential of − 1.5 V for 150 s. After standing for 5 s, SWV was scanned from -1.2 V to 0.2 V while reduction of the deposited metal into metal ions and the anodic dissolution peak of Cd^{2+}. After each analysis, the electrode surface was cleaned for 120 s at a potential of 1.0 V. The deposition potential and deposition time and solution parameters were optimized specifically for our electrode system before any measurements.

Results and discussion

The morphology and structure characterization of a-g-C_3N_4

Figure 1 shows the SEM and TEM electrographs of the b-g-C_3N_4 samples fabricated by thermal polycondensation. The a-g-C_3N_4 exhibits gauze-like 2D nanosheets with irregularly block morphology. The 2D layers show reduced thickness, which may result due to the destruction of large structures during ultrasonication and protonation. The TEM electrographs in Fig. 1c, d show a-g-C_3N_4 irregular nanosheets which corroborate well with the observed SEM morphologies. The newly fabricated near transparent lamellar a-g-C_3N_4 structures resemble graphene [25]. Our data confirm the successful fabrication of g-C_3N_4 nanosheets.

Figure 2 shows the X-ray diffractograms of b-g-C_3N_4 and a-g-C_3N_4 nanosheets. In both substrates, the intense peak at 31.8° corresponds to (002) plane [26]. The appearance of (100) plane is confirmed by the presence of a peak at 13.2°. The intensity of both peaks decreased from b-g-C_3N_4 to a-g-C_3N_4 nanosheets. However, the XRD signatures of the b-g-C_3N_4 to a-g-C_3N_4 did not vary, which conforms the presence of base a-g-C_3N_4 structures in both materials. According to the Scherrer formula, the calculated crystallite sizes of b-g-C_3N_4 and a-g-C_3N_4 are about 15 nm and 11 nm, respectively [27, 28]. The FTIR spectrums of b-g-C_3N_4 and a-g-C_3N_4 nanosheets are similar. In agreement with XRD data, the

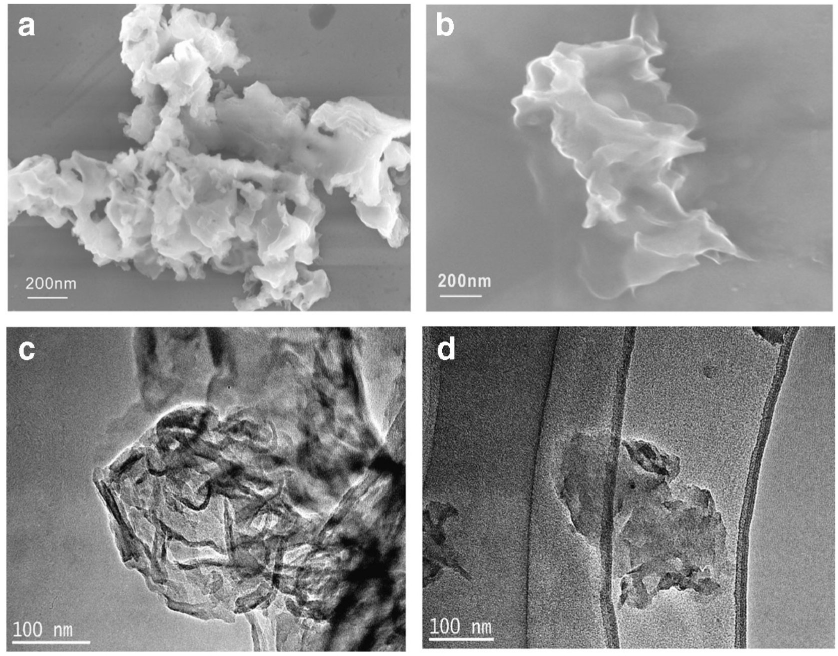

Fig. 1 SEM and TEM images of b-g-C_3N_4 (**a**, **c**) and a-g-C_3N_4 (**b**, **d**)

FTIR data confirm that ultrasonication and protonation did not destruct base b-g-C_3N_4 structure [22]. The sharp band appears at 809 cm^{-1} relates to the *s*-triazine ring vibrations. The bands in the range of 900~1800 cm^{-1} are derived from the CN heterocyclic structure. The broad band in the range of 3200~3400 cm^{-1} is due to stretching vibrations of absorption -NH or -NH_2 groups [29, 30]. The Cd^{2+} interactions with both b-g-C_3N_4 and a-g-C_3N_4 were also examined, and the spectral results are shown in the Electronic Supplementary Material (ESM, Fig. S1). The EDX data evidence the presence of Cd^{2+} on a-g-

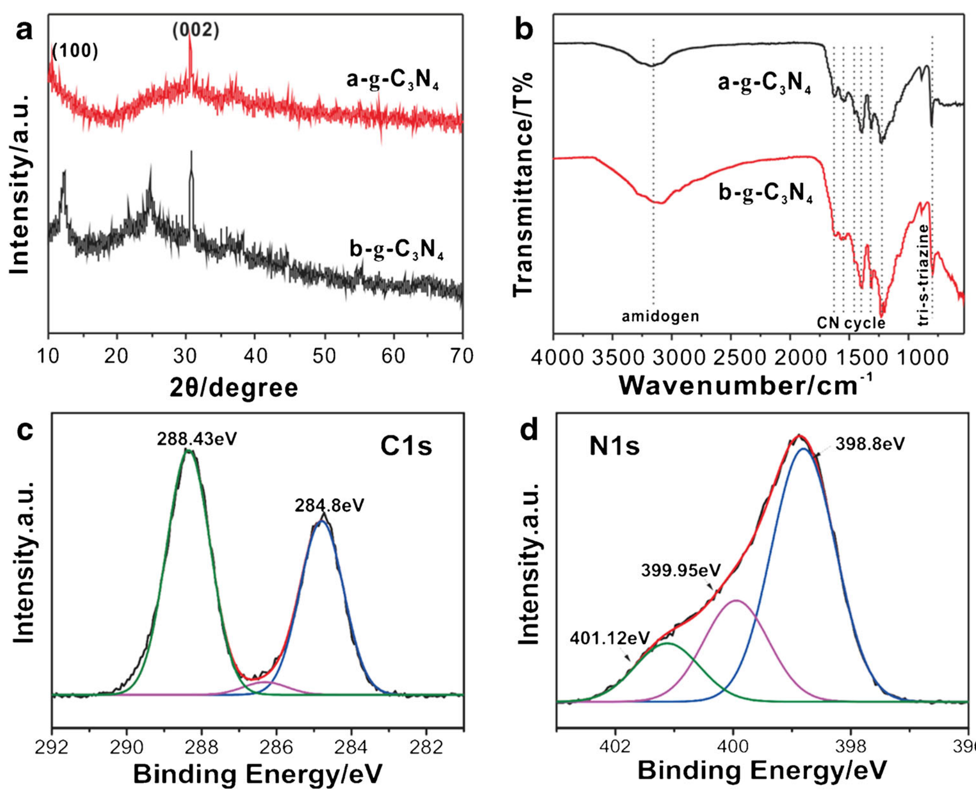

Fig. 2 XRD patterns (**a**) and FTIR spectra (**b**) of b-g-C_3N_4 and a-g-C_3N_4; XPS spectra of (**c**) C1s and (**d**) N1s of a-g-C_3N_4

C_3N_4 used for sensor electrode fabrications. The shift of 2800 cm^{-1} band shows an intimate association of Cd^{2+} with OH groups on C_3N_4 surface sites. FTIR signatures around -OH group bands showed marked variations upon Cd^{2+} addition on a-g-C_3N_4 [31].

The chemical state of elements on C_3N_4 substrates at the near surface, particularly C and N is also determined by X-ray photoelectron spectroscopy (XPS). As shown in Fig. 2c, in agreement with previous work [32], the C_{1s} peak at 288.34 eV is due to sp^2 hybridized aromatic C. The characterized peak at 284.8 eV corresponds to graphene-like structure [33]. Three peaks at binding energies of 401.12, 399.95, and 398.8 eV, respectively, are observed in the N 1s spectrum. The intense peak at 398.7 eV is derived from the N attached to the graphite carbon. The peak at 399.95 eV assigns due to the bridging of N in N-$(C)_3$ [34–36]. A very weak peak at 401.12 eV is due to charging, or charge localization in heterocycles and canon of N_3 atomic moiety.

CV and EIS characterization of a-g-C_3N_4-modified GCE

The electron transfer rates of the newly prepared a-g-C_3N_4 and b-g-C_3N_4-modified GCE electrodes, i.e., hereafter a-g-C_3N_4 and b-g-C_3N_4 GCE, respectively, were determined electrochemically using cyclic voltammograms (CV) and electrochemical impedance spectroscopy (EIS) in 5 mM Fe $(CN_6)^{3-/4-}$ and 0.1 M KCl solution at a 100-mV/s scanning rate. As shown in Fig. 3a, when compared to bare GCE, the current intensity of the modified electrodes is weakened due to inhibited electron transfer [37]. The CV current density of a-g-C_3N_4-modified electrode is higher than that of b-g-C_3N_4 electrode. Due to high specific surface area and conductivity, the a-g-C_3N_4 show enhanced electron transfer rates across the interface. Figure 3b shows the EIS spectra obtained using b-g-C_3N_4 and a-g-C_3N_4-modified GCE and bare GCEe in Fe $(CN_6)^{3-/4-}$ redox system. In a typical EIS spectrum, the circular and linear segments reflect high frequency electron transfer resistance (R_{et}) and low frequency diffusion, respectively. The R_{et} values of the electrode vary in the following order: $R_{et}^{bulk} > R_{et}^{nanosheet} >> R_{et}^{bare}$. When compared to GCE, R_{et} values of the a-g-C_3N_4-modified electrodes are larger. Several conclusions can be drawn: (i) the nanomaterials are attached onto electrodes successfully and (ii) the semicircle portion corresponds to the electron transfer resistance at high frequencies and a linear portion reflecting the diffusion process at low frequencies. The modified electrodes possess semicircles with large curvature than bare GCE, representing that the R_{et} values of b-g-C_3N_4 and a-g-C_3N_4 nanosheets are bigger. This suggested that the nanomaterials have been successfully assembled on the electrode surface. Besides, the smaller R_{et} value of a-g-C_3N_4/GCE when compared to b-g-C_3N_4/GCE implies enhanced electron transfer properties of a-g-C_3N_4 activated by exfoliation and protonation [37]. These results are consistent with the CV data shown in Fig. 3a.

Optimization of experimental parameters

The performance of Cd^{2+} detection by a-g-C_3N_4 and b-g-C_3N_4 GC electrodes was assessed under SWASV mode. The Cd^{2+} detection experiments were performed in 0.1 M acetate buffer (pH 5.00) with − 1.5 V depositional potential. As shown in Fig. 4, when compared to bare GCE, the highest peak current is observed with a-g-C_3N_4 GCE sensor.

Performance of Cd^{2+} detection by a-g-C_3N_4-modified GCE electrode was optimized by varying experimental parameters as supporting electrolyte, pH, deposition potential, and deposition time. Figure 5a shows the variation of stripping current of a-g-C_3N_4 GCE for 5 μM Cd^{2+} in 0.1 M NH_4Cl-HCl, NaAc-HAc, and PBS at pH 5.0. The a-g-C_3N_4 GCE shows the highest stripping current in 0.1 M NaAc-HAc buffer. The solution pH also exerts a significant effect on the Cd^{2+} stripping current. In our experiments, a maximal stripping current is noted when solution pH 5.0, where over 95% of cadmium occurs as free Cd^{2+} species. At high acid conditions, the competition between H^+ and Cd^{2+} towards the sensor is apparent. Both deposition potential and time also play a vital

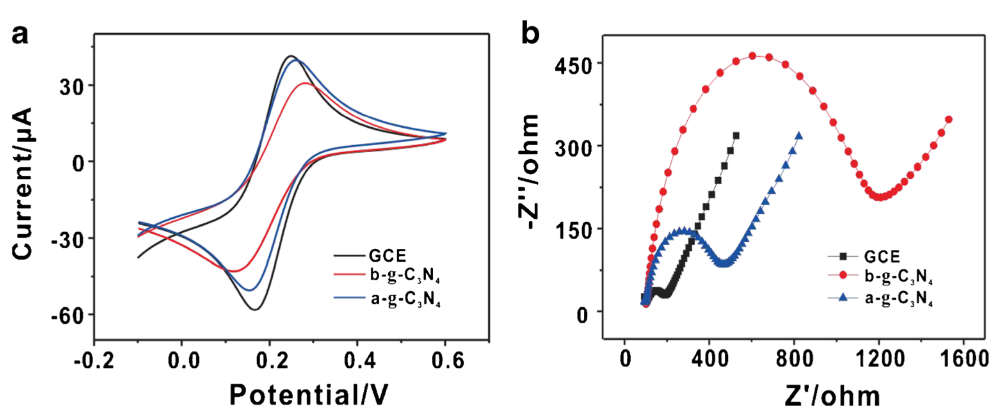

Fig. 3 The cyclic voltammetry current curves of 5 mM $Fe(CN_6)^{3-/4-}$ (**a**) and electrochemical impedance spectra (**b**) of bare GCE, b-g-C_3N_4/GCE, and a-g-C_3N_4 /GCE

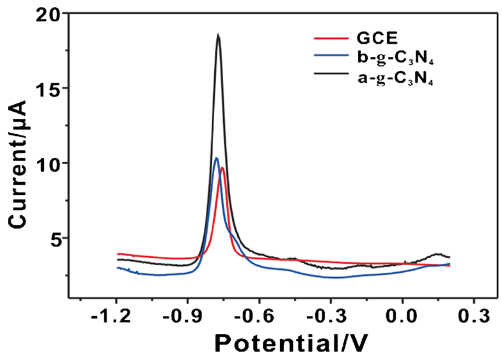

Fig. 4 The stripping responses toward 0.5 μM Cd^{2+} in 0.1 M acetate buffer solution (pH 5.0) under four different electrodes. Deposition potential, − 1.5 V; deposition time, 120 s

role in metal accumulation on the electrode surface. Variation of stripping current as a function of depositional potential for 0.5 μM Cd^{2+} in 0.1 M NaAc-HAc at pH 5.00 is shown in Fig. 5. The deposition reaches a plateau around − 1.5 V deposition potential. When deposition potential < − 1.5 V, Cd^{2+} tends to deposit on the electrode with evolution of H_2 passivating the electrode surface. In a separate experiment, the deposition time was varied while keeping other parameters fixed at optimized values. The stripping current for 0.5 μM Cd^{2+} shows a monotonous increase reaching a breaking point around 150 s.

After the breakpoint, the deposition time shows a decline. The 150 s deposition time was chosen as optimal for 0.5 μM Cd^{2+} deposition. Based on the results obtained so far, a solution with following base conditions was used in developing a sensitive Cd^{2+} detection method at ambient room temperature: pH 5 0.1 M NaAc-HAc buffer, deposition potential − 1.5 V, deposition time 150 s, step potential 5 mV, amplitude 25 mV, and frequency 25 Hz.

Electrochemical detection of Cd^{2+} with a-g-C_3N_4-modified GCE by SWASV method

To determine Cd^{2+} in environmental samples, as shown in Fig. 6, a calibration curve in the range 0.05~0.7 μM is developed using a-g-C_3N_4 and b-g-C_3N_4 sensor by the electrochemical method under SWASV mode from the data received for method opitmization. The relationship between stripping current vs. Cd^{2+} is linear, i.e., I/μA = − 0.265 + 22.668 C/μA/μM (R^2 = 0.986), and, i.e., I/μA = − 0.463 + 12.792 C/μA/μM (R^2 = 0.991), with limit of detection (LOD) of 0.00394 μM and 0.00703 μM, respectively. Compared with theb-g-C_3N_4-modified electrode, the a-g-C_3N_4-modified electrode displays higher sensitivity and lower detection limit. As shown in Table 1, the sensing electrode material was coated with different materials to gain enhanced LOD and sensitivity for metal ions detection. As always, it is important to promote environmentally benign substrates for electrode modification experiments. Therefore, we compared our data with graphite-based electrode modification data. Our method shows comparable or slightly better sensitivity when compared to published data [41].

Fig. 5 Optimum experimental conditions. Influence of **a** supporting electrolytes, **b** pH value, **c** Deposition potential, and **d** Deposition time on the voltammetric responses of the a-g-C_3N_4 /GCE. Data were evaluated by SWASV of 0.5 μM Cd^{2+}

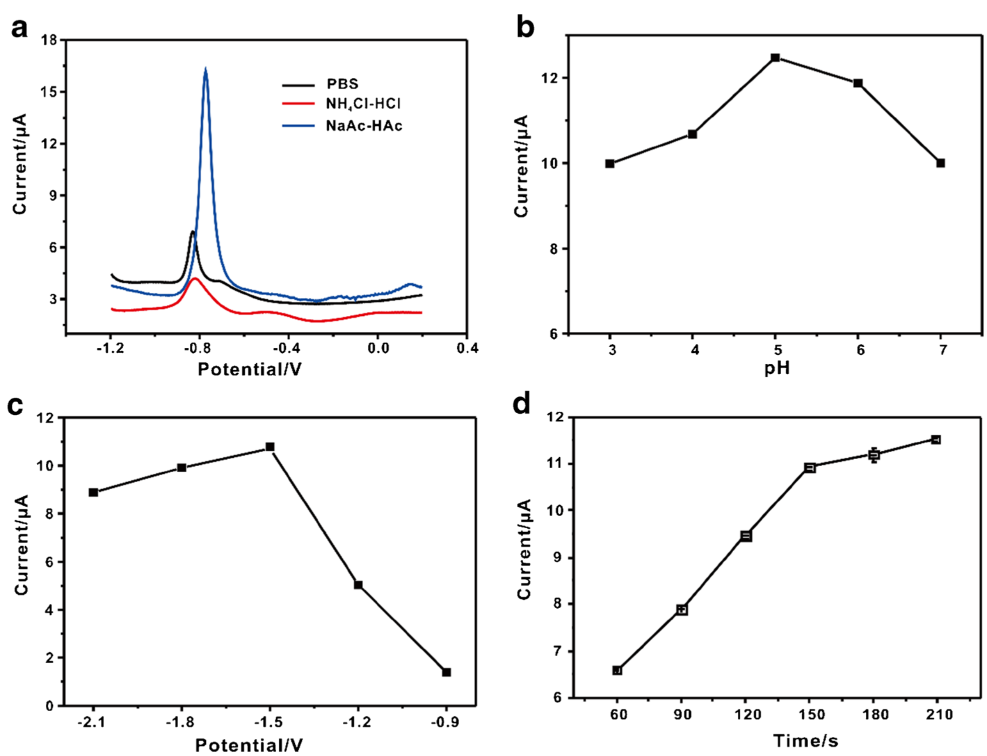

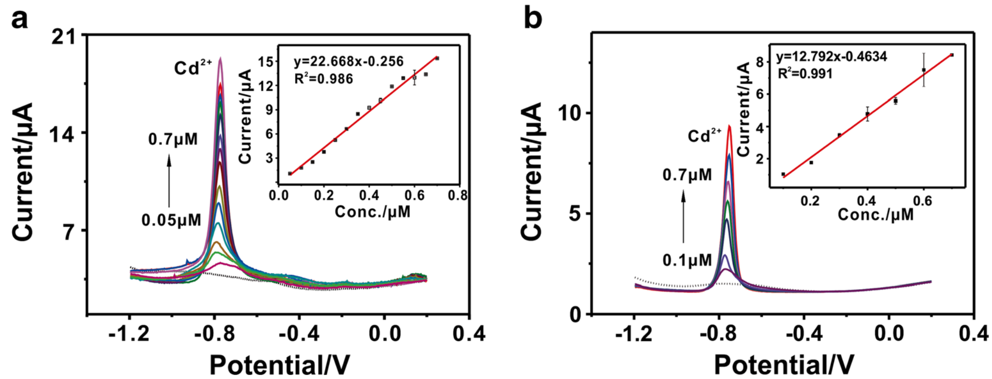

Fig. 6 SWASV responses and the corresponding error bars (in the inset) of the a-g-C_3N_4-modified GCE (**a**) and the b-g-C_3N_4-modified GCE (**b**)

In separate experiments (see ESM Fig. S2), the performance of bare GCE and ultrasonically exfoliated g-C_3N_4 (ult-g-C_3N_4) was also examined for Cd^{2+}. As always, bare GCE showed poor sensitivity. When the electrode is modified with a-g-C_3N_4, the sensitivity was enhanced reaching an optimal value for determination of Cd^{2+}. This result attributes to the a-g-C_3N_4 ultrathin layer and high surface for the effective accumulation of metal ions required for enhanced sensitivity.

To confirm the data, the active surface area of the electrode material was determined using CV technique for 1 mM $Fe(CN_6)^{3-/4-}$ with 0.1 M KCl at different scan rates. Figure S3 (see the ESM) shows a linear relationship between I_p and $v^{1/2}$ based on Randles–Sevcik formula [44, 45]: $I_p = 2.69 \times 10^5 n^{3/2} AD^{1/2} v^{1/2} C_0$, where A is the real area of the electrode (cm^2), D is the diffusion coefficient (cm^2/s), C_0 is the concentration of the $K_3Fe(CN_6)$ (mol/cm^3). For the utilized electrolyte, $n = 1$ and $D = 7.6 \times 10^{-6}$ cm^2/s [46]. The active surface areas were calculated from the slope of the $I_p - v^{1/2}$ plots. The highest surface area was reported for a-g-C_3N_4 GCE as 0.0141 cm^2. In agreement with previous data [47], the calculation details for other electrode materials are shown in Table S1 (see ESM).

Possible adsorption mechanism of Cd^{2+}

To explore the influences of exfoliation and protonation treatment, the interactions between Cd^{2+} and b-g-C_3N_4 and a-g-C_3N_4 were investigated by adsorption experiments. Figure 7 shows the XPS spectral comparisons of b-g-C_3N_4 and a-g-C_3N_4 after Cd^{2+} adsorption. The binding energy of Cd^{2+} adsorbed on b-g-C_3N_4 and a-g-C_3N_4 nanosheets both shift in negative direction as opposed to purified $Cd(NO_3)_2$ (Fig. 7a). The shift illustrates that there are strong chemical interactions between Cd^{2+} and b-g-C_3N_4/a-g-C_3N_4. The binding energy of a-g-C_3N_4 shifts negatively more than b-g-C_3N_4, indicating the stronger interaction of the Cd^{2+} which enhances electrochemical detection [47]. The broader peak of the Cd 3d after adsorption indicates that the chemical environment in the vicinity of Cd^{2+} has perturbed [48]. Figure 7b shows the N1s spectra of a-g-C_3N_4, b-g-C_3N_4/Cd, and a-g-C_3N_4/Cd. The N1s spectra peaks of N-C=N, N-(C_3), C-N-H have shifted due to interactions between N and Cd^{2+}. Furthermore, the area ratio of the three peaks of the b-g-C_3N_4/Cd^{2+}(1:0.26:0.18) and a-g-C_3N_4 /Cd^{2+} (1:0.24:0.16) compared to a-g-C_3N_4 (1:0.41:0.23) were remarkably changed, which is mainly due to the interaction between Cd^{2+} and potential adsorption sites of the presence of N-(C_3) and C-N-H [16]. As shown in the Fig. 7c, the main peak of carbon has shifted 0.04 eV owing to significant interaction between Cd and C. This might be due to the flowing electrons existing in the sp2 carbon which provides an adsorption site for Cd^{2+} [16].

Table 1 The sensitivity and LOD values toward Cd^{2+} with different electrodes by SWASV method

Electrodes	Sensitivity	LOD	Ref
Pd@PAC/GCE	0.1059 μA/nM	13.33 nM	[38]
rGO/CMC/GSH/GCE	4.5 μA/nM	0.05 nM	[39]
Fe_3O_4-chitosan/GCE	8.11 μA/μM	3.92 μM	[40]
MgFe-LDH/graphene/GCE	26.15 μA /μM	4.7 nM	[41]
GO/κ-Car/l-Cys/GCE	1.39 μA/nM	0.58 nM	[42]
ZnO NF/GCE	~	1.8 nM	[43]
g-C_3N_4 nanosheet/GCE	22.668 μA /μM	3.97 nM	This paper

Interference measurements

The chemical interference from metal ions present in the matrix is a major limiting factor in the application of electrochemical methods for routine analysis. The interference of Cu^{2+}, Pb^{2+}, and Hg^{2+} on Cd^{2+} detection by SWASV was examined using both single and multi-elements matrix samples. For single element matrix, the interference of Cu^{2+} and Hg^{2+} on Cd^{2+} detection was examined, whereas in multi-element mode interference of Cu^{2+}, Hg^2, and Pb^{2+} on Cd^{2+} detection was examined. Optimized parameters as results during method development were used. Figure 8 shows the effects of Hg^{2+} or Cu^{2+} and Hg^{2+}, Cu^{2+}, and Pb^{2+} on Cd^{2+}

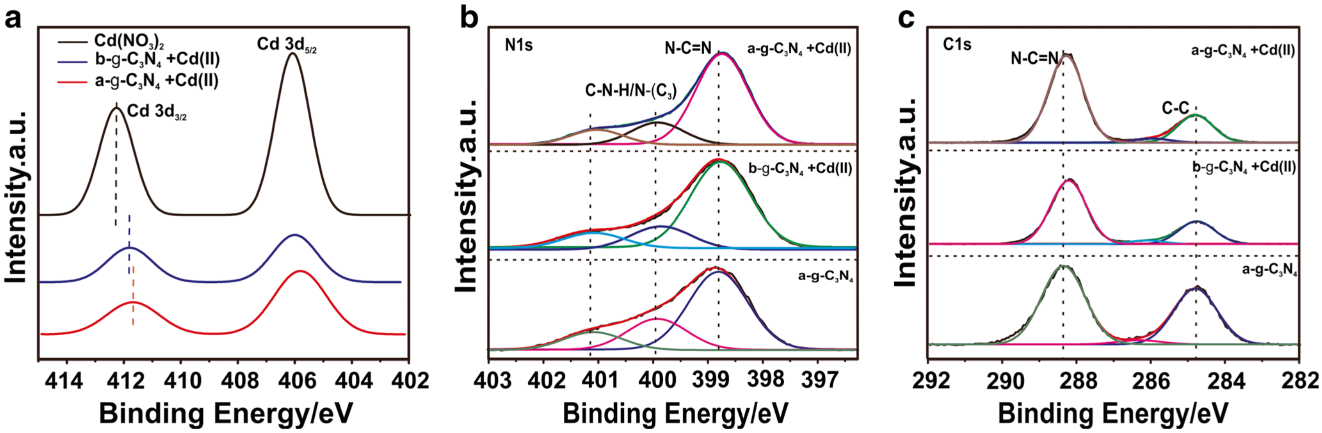

Fig. 7 The high solution XPS of b-g-C_3N_4 and a-g-C_3N_4 before adsorption and after adsorption. a) Cd 3d; b) N1 s; c) C1s

detection. We observe that the peak currents of Cd^{2+} increased and the peaks of Cu^{2+} and Hg^{2+} showed no variation with the Cd^{2+} addition (Fig. 8a, b). The sensitivity values for Cd^{2+} in the presence of Cu or Hg were 22.51 μA/μM or 22.546 μA/μM, respectively, which show their minimal interference on Cd^{2+} peak. The a-g-C_3N_4-modified electrode avoids interference between Cu^{2+} and Cd^{2+}. The metal ion binding sites on a-g-C_3N_4 nanosheets showed no competition between Cd^{2+} and Hg^{2+} or Cu^{2+} [9].

As expected, when Cu^{2+}, Pb^{2+}, and Hg^{2+} coexist with Cd^{2+}, the Cd^{2+} detection sensitivity did not change significantly. During the simultaneous analysis of all of the four ions coexisting in the solution, however, there is an obvious tendency that the peak currents of Hg^{2+} and Pb^{2+} are enhanced due to mutual promotion of Hg^{2+} and Pb^{2+} during the accumulation [49, 50]. The Cd^{2+} detection sensitivity in multi-element matrix samples shows no change, which shows that the a-g-C_3N_4 GCE robust can be used as a multi-element detection.

Fig. 8 Variation of current vs. potential in the presences of other metal ions under SWASV mode using a-g-C_3N_4-modified GCE. Cd^{2+} concentration range 0.1–1.0 μM in **a** 0.5 μM Cu^{2+}, **b** 0.5 μM Hg^{2+}, **c** 0.5 μM Hg^{2+}, 0.5 μM Pb^{2+}, and 0.5 μM Cu^{2+}. The inset shows Cd^{2+} calibration curves in the presence of foreign metal ions

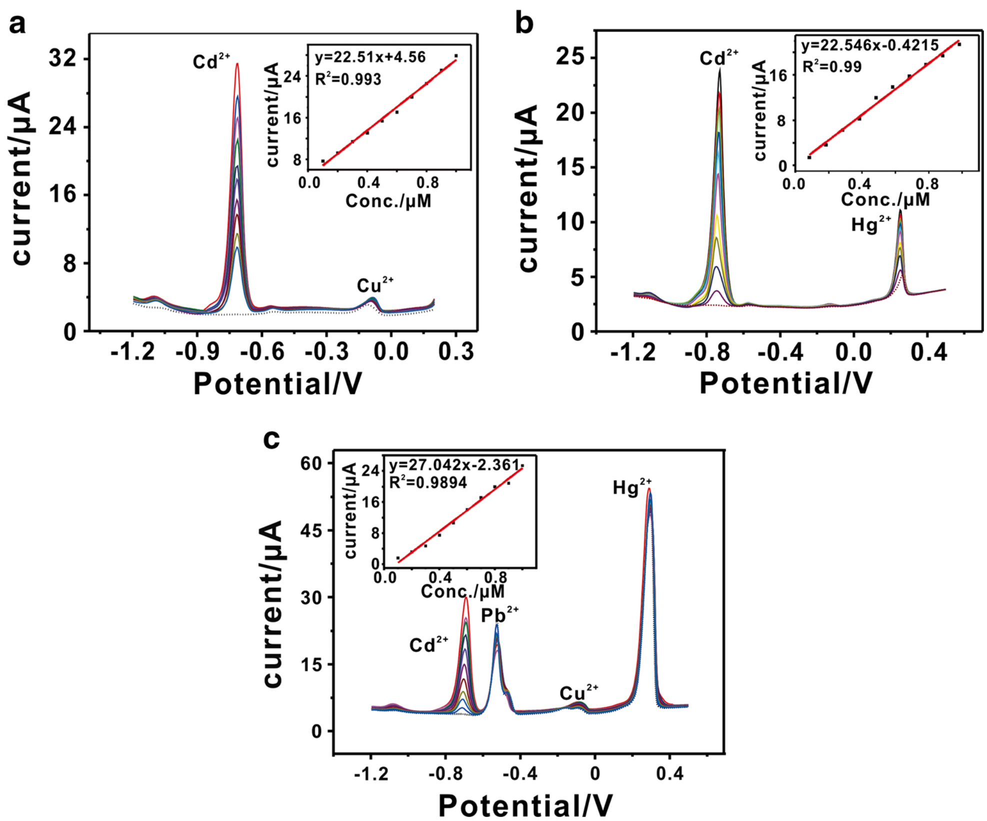

Analysis of rice and natural water samples

Finally, our a-g-C_3N_4 GCE was used for the detection of Cd^{2+} in rice and natural water by standard addition. The standard addition curves obtained for rice and natural water are shown in Figs. S4 and S5 (see the ESM), respectively. For the digested rice sample, the sensitivity value calculated from the data is 8.083 μA/mg/kg (18.18 μA/μM). The LOD value is 0.017 mg/kg, which is lower than the recommended value by WHO, viz. 0.2 mg/kg. The lake water sample taken from the Hubing Lake in Hefei University of Technology, China, was filtered through a 0.02-μm membrane followed by 1:9 dilution with 0.1 M HAc-NaAc before Cd^{2+} analysis. The standard addition plot is shown in Fig. S5 (see the ESM). The sensitivity and LOD values are 17.02 μA/μM and 0.00522 μM. Spike recovery carried out with 0.01 μM Cd^{2+} was 1 ± 10%. In both cases, the potential of using a-g-C_3N_4 GCE in metal detection is evident.

Conclusions

The a-g-C_3N_4 with nanosheets were fabricated by thermal polycondensation of urea, by ultrasonic exfoliation, and followed by protonation. The newly prepared glassy carbon electrode was used for electrochemical Cd^{2+} detection with of 22.668 μA/μM sensitivity and LOD 0.00394 μM. The a-g-C_3N_4 GCE is interference free that can be employed for multi-element detection of environmental samples such as food and natural water. The activated treatment cannot only improve the specific area of a-g-C_3N_4 nanosheets but also create more active sites for adsorption of heavy metal ions.

Acknowledgments The authors acknowledge the financial support from the National Natural Science Foundation of China (Grant No. 21777164), National Basic Research Program of China (Grant No. SQ2019YFC040023), Fundamental Research Funds for the Central Universities (Grant No. PA2019GDQT0019 and PA2019GDQT0017), and Key Technologies R & D Program of Anhui Province (No. 1704c0402195). R. W. acknowledges the Program of Distinguished Professor in B&R Countries (Grant No. DL20180052).

Compliance with ethical standards

Conflict of interest The authors declare that they have no competing interests.

References

1. Wu Y, Pang H, Liu Y, Wang X, Yu S, Fu D, et al. Environmental remediation of heavy metal ions by novel-nanomaterials: a review. Environ Pollut. 2019;246:608–20. https://doi.org/10.1016/j.envpol.2018.12.076.
2. Teodoro KBR, Migliorini FL, Facure MHM, Correa DS. Conductive electrospun nanofibers containing cellulose nanowhiskers and reduced graphene oxide for the electrochemical detection of mercury(II). Carbohydr Polym. 2019;207:747–54. https://doi.org/10.1016/j.carbpol.2018.12.022.
3. Polykretis P, Cencetti F, Donati C, Luchinat E, Banci L. Cadmium effects on superoxide dismutase 1 in human cells revealed by NMR. Redox Biol. 2019;21:101102. https://doi.org/10.1016/j.redox.2019.101102.
4. Xiong R, Wu Q, Trbojevich R, Muskhelishvili L, Davis K, Bryant M, et al. Disease-related responses induced by cadmium in an in vitro human airway tissue model. Toxicol Lett. 2019;303:16–27. https://doi.org/10.1016/j.toxlet.2018.12.009.
5. Yang P, Zhou R, Zhang W, Yi R, Tang S, Guo L, et al. High-sensitivity determination of cadmium and lead in rice using laser-induced breakdown spectroscopy. Food Chem. 2019;272:323–8. https://doi.org/10.1016/j.foodchem.2018.07.214.
6. Li J, Guo S, Zhai Y, Wang E. High-sensitivity determination of lead and cadmium based on the Nafion-graphene composite film. Anal Chim Acta. 2009;649(2):196–201. https://doi.org/10.1016/j.aca.2009.07.030.
7. Kitte SA, Li S, Nsabimana A, Gao W, Lai J, Liu Z, et al. Stainless steel electrode for simultaneous stripping analysis of Cd(II), Pb(II), Cu(II) and Hg(II). Talanta. 2019;191:485–90. https://doi.org/10.1016/j.talanta.2018.08.066.
8. Zhao G, Liu G. Synthesis of a three-dimensional (BiO)2CO3@single-walled carbon nanotube nanocomposite and its application for ultrasensitive detection of trace Pb(II) and Cd(II) by incorporating Nafion. Sensors Actuators B Chem. 2019;288:71–9. https://doi.org/10.1016/j.snb.2019.02.106.
9. Lin C-H, Li P-H, Yang M, Ye J-J, Huang X-J. Metal replacement causing interference in stripping analysis of multiple heavy metal analytes: kinetic study on Cd(II) and Cu(II) electroanalysis via experiment and simulation. Anal Chem. 2019. https://doi.org/10.1021/acs.analchem.9b01724.
10. Xie Y-L, Zhao S-Q, Ye H-L, Yuan J, Song P, Hu S-Q. Graphene/CeO 2 hybrid materials for the simultaneous electrochemical detection of cadmium(II), lead(II), copper(II), and mercury(II). J Electroanal Chem. 2015;757:235–42. https://doi.org/10.1016/j.jelechem.2015.09.043.
11. Wu X, Wu S, Li Y, Chen H, Yuan Q, Gan W. A highly sensitive electrochemical sensor for Cd(II) based on protic salt derived nitrogen and sulfur co-doped porous carbon. Anal Chim Acta. 2019;1046:115–22. https://doi.org/10.1016/j.aca.2018.09.030.
12. Awual MR, Khraisheh M, Alharthi NH, Luqman M, Islam A, Rezaul Karim M, et al. Efficient detection and adsorption of cadmium(II) ions using innovative nano-composite materials. Chem Eng J. 2018;343:118–27. https://doi.org/10.1016/j.cej.2018.02.116.
13. Yu XY, Meng QQ, Luo T, Jia Y, Sun B, Li QX, et al. Facet-dependent electrochemical properties of Co3O4 nanocrystals toward heavy metal ions. Sci Rep. 2013;3:2886. https://doi.org/10.1038/srep02886.
14. Yang M, Jiang T-J, Guo Z, Liu J-H, Sun Y-F, Chen X, et al. Sensitivity and selectivity sensing cadmium(II) using amination functionalized porous SnO 2 nanowire bundles-room temperature ionic liquid nanocomposite: combined efficient cation capture with control experimental conditions. Sens Actuators B: Chem. 2017;240:887–94. https://doi.org/10.1016/j.snb.2016.09.060.
15. Zhang S, Liu Y, Gu P, Ma R, Wen T, Zhao G, et al. Enhanced photodegradation of toxic organic pollutants using dual-oxygen-doped porous g-C3N4: mechanism exploration from both experimental and DFT studies. Appl Catal B Environ. 2019;248:1–10. https://doi.org/10.1016/j.apcatb.2019.02.008.
16. Cai X, He J, Chen L, Chen K, Li Y, Zhang K, et al. A 2D-g-C3N4 nanosheet as an eco-friendly adsorbent for various environmental pollutants in water. Chemosphere. 2017;171:192–201. https://doi.org/10.1016/j.chemosphere.2016.12.073.

17. Shen C, Chen C, Wen T, Zhao Z, Wang X, Xu A. Superior adsorption capacity of g-C(3)N(4) for heavy metal ions from aqueous solutions. J Colloid Interface Sci. 2015;456:7–14. https://doi.org/10.1016/j.jcis.2015.06.004.
18. Hatamie A, Jalilian P, Rezvani E, Kakavand A, Simchi A. Fast and ultra-sensitive voltammetric detection of lead ions by two-dimensional graphitic carbon nitride (g-C3N4) nanolayers as glassy carbon electrode modifier. Measurement. 2019;134:679–87. https://doi.org/10.1016/j.measurement.2018.10.082.
19. Wang M, Fu R, Jin CY, Li ZL, Sun J, Yu P, et al. The facile fabrication of g-C3N4 ultrathin nanosheets with higher specific surface areas for highly sensitive detection of trace cadmium. Measurement. 2019;140:548–56. https://doi.org/10.1016/j.measurement.2019.03.067.
20. Xu TG, Zhang C, Shao X, Wu K, Zhu YF. Monomolecular-layer Ba5Ta4O15 nanosheets: synthesis and investigation of photocatalytic properties. Adv Funct Mater. 2006;16(12):1599–607. https://doi.org/10.1002/adfm.200500849.
21. Yongfu S, Hao C, Shan G, Zhihu S, Qinghua L, Qin L, et al. Freestanding tin disulfide single-layers realizing efficient visible-light water splitting. Angew Chem. 2012;51(35):8668.
22. Zhang YJ, Thomas A, Antonietti M, Wang XC. Activation of carbon nitride solids by protonation: morphology changes, enhanced ionic conductivity, and photoconduction experiments. J Am Chem Soc 131 (1):50-+. 2009. https://doi.org/10.1021/ja808329f.
23. Wang L, Xu WH, Yang R, Zhou T, Hou D, Zheng X, et al. Electrochemical and density functional theory investigation on high selectivity and sensitivity of exfoliated nano-zirconium phosphate toward lead(II). Anal Chem. 2013;85(8):3984–90. https://doi.org/10.1021/ac3037014.
24. Jiang T-J, Guo Z, Ma M-J, Fang L, Yang M, Li S-S, et al. Electrochemical laser induced breakdown spectroscopy for enhanced detection of Cd(II) without interference in rice on layer-by-layer assembly of graphene oxides. Electrochim Acta. 2016;216:188–95. https://doi.org/10.1016/j.electacta.2016.09.016.
25. Geim AK, Novoselov KS. The rise of graphene. Nat Mater 6 (3): 183-191. doi:DOI. 2007. https://doi.org/10.1038/nmat1849.
26. Pattadar DK, Sharma JN, Mainali BP, Zamborini FP. Anodic stripping electrochemical analysis of metal nanoparticles. Curr Opin Electrochem. 2019;13:147–56. https://doi.org/10.1016/j.coelec.2018.12.006.
27. Dastan D, Panahi SL, Chaure NB. Characterization of titania thin films grown by dip-coating technique. J Mater Sci-Mater Electron. 2016;27(12):12291–6. https://doi.org/10.1007/s10854-016-4985-4.
28. Dastan D. Effect of preparation methods on the properties of titania nanoparticles: solvothermal versus sol-gel. Appl Phys A-Mater Sci Process. 2017;123(11):13. https://doi.org/10.1007/s00339-017-1309-3.
29. Joshi RK, Carbone P, Wang FC, Kravets VG, Su Y, Grigorieva IV, et al. Precise and ultrafast molecular sieving through graphene oxide membranes. Science. 2014;343(6172):752–4. https://doi.org/10.1126/science.1245711.
30. Kim HW, Yoon HW, Yoon SM, Yoo BM, Ahn BK, Cho YH, et al. Selective gas transport through few-layered graphene and graphene oxide membranes. Science. 2013;342(6154):91–5. https://doi.org/10.1126/science.1236098.
31. Shehzad K, Ahmad M, Xie C, Zhan D, Wang W, Li Z, et al. Mesoporous zirconia nanostructures (MZN) for adsorption of As(III) and As(V) from aqueous solutions. J Hazard Mater. 2019;373:75–84. https://doi.org/10.1016/j.jhazmat.2019.01.021.
32. Yang SB, Feng XL, Wang XC, Mullen K. Graphene-based carbon nitride nanosheets as efficient metal-free electrocatalysts for oxygen reduction reactions. Angew Chem Int Ed. 2011;50(23):5339–43. https://doi.org/10.1002/anie.201100170.
33. Yang SB, Gong YJ, Zhang JS, Zhan L, Ma LL, Fang ZY, et al. Exfoliated graphitic carbon nitride nanosheets as efficient catalysts for hydrogen evolution under visible light. Adv Mater. 2013;25(17):2452–6. https://doi.org/10.1002/adma.201204453.
34. Martha S, Nashim A, Parida KM. Facile synthesis of highly active g-C3N4 for efficient hydrogen production under visible light. J Mater Chem A. 2013;1(26):7816–24. https://doi.org/10.1039/c3ta10851a.
35. Kumar S, Baruah A, Tonda S, Kumar B, Shanker V, Sreedhar B. Cost-effective and eco-friendly synthesis of novel and stable N-doped ZnO/g-C3N4 core-shell nanoplates with excellent visible-light responsive photocatalysis. Nanoscale. 2014;6(9):4830–42. https://doi.org/10.1039/c3nr05271k.
36. Vinu A. Two-dimensional hexagonally-ordered mesoporous carbon nitrides with tunable pore diameter, surface area and nitrogen content. Adv Funct Mater. 2008;18(5):816–27. https://doi.org/10.1002/adfm.200700783.
37. Zhang J, Zhu Z, Di J, Long Y, Li W, Tu Y. A sensitive sensor for trace Hg2+ determination based on ultrathin g-C3N4 modified glassy carbon electrode. Electrochim Acta. 2015;186:192–200. https://doi.org/10.1016/j.electacta.2015.10.173.
38. Ting Zhanga HJ, Fanga Y, Guana JB. Detection of trace Cd2+, Pb2+ and Cu2+ ions via porous activated carbon supported palladium nanoparticles modified electrodes using SWASV.pdf. Mater Chem Phys. 2019;225:433–42. https://doi.org/10.1016/j.matchemphys.2019.01.010.
39. Priya T, Dhanalakshmi N, Thennarasu S, Thinakaran N. Ultra sensitive detection of Cd (II) using reduced graphene oxide/carboxymethyl cellulose/glutathione modified electrode. Carbohydr Polym. 2018;197:366–74. https://doi.org/10.1016/j.carbpol.2018.06.024.
40. Zhou S-F, Han X-J, Liu Y-Q. SWASV performance toward heavy metal ions based on a high-activity and simple magnetic chitosan sensing nanomaterials. J Alloys Compd. 2016;684:1–7. https://doi.org/10.1016/j.jallcom.2016.05.152.
41. Ma Y, Wang Y, Xie D, Gu Y, Zhu X, Zhang H, et al. Hierarchical MgFe-layered double hydroxide microsphere/graphene composite for simultaneous electrochemical determination of trace Pb(II) and Cd(II). Chem Eng J. 2018;347:953–62. https://doi.org/10.1016/j.cej.2018.04.172.
42. Priya T, Dhanalakshmi N, Thennarasu S, Thinakaran N. A novel voltammetric sensor for the simultaneous detection of Cd(2+) and Pb(2+) using graphene oxide/kappa-carrageenan/l-cysteine nanocomposite. Carbohydr Polym. 2018;182:199–206. https://doi.org/10.1016/j.carbpol.2017.11.017.
43. Liu J, Zhu G, Chen M, Ma X, Yang J. Fabrication of electrospun ZnO nanofiber-modified electrode for the determination of trace Cd(II). Sens Actuators B: Chem. 2016;234:84–91. https://doi.org/10.1016/j.snb.2016.04.073.
44. Wei SH, Zhao FQ, Xu ZY, Zeng BZ. Voltammetric determination of folic acid with a multi-walled carbon nanotube-modified gold electrode. Microchim Acta. 2006;152(3-4):285–90. https://doi.org/10.1007/s00604-005-0437-1.
45. Yu X, Mai Z, Xiao Y, Zou X. Electrochemical behavior and determination of L-tyrosine at single-walled carbon nanotubes modified glassy carbon electrode. Electroanalysis. 2008;20(11):1246–51. https://doi.org/10.1002/elan.200704179.
46. Hatamie A, Echresh A, Zargar B, Nur O, Willander M. Fabrication and characterization of highly-ordered zinc oxide nanorods on gold/glass electrode, and its application as a voltammetric sensor. Electrochim Acta. 2015;174:1261–7. https://doi.org/10.1016/j.electacta.2015.06.083.
47. Sun YF, Jian W, Li PH, Yang M, Huang XJ. Highly sensitive electrochemical detection of Pb(II) based on excellent adsorption and surface Ni(II)/Ni(III) cycle of porous flower-like NiO/rGO

nanocomposite. Sens Actuator B-Chem. 2019;292:136–47. https://doi.org/10.1016/j.snb.2019.04.131.
48. Xiao XY, Chen SH, Li SS, Wang J, Zhou WY, Huang XJ. Synergistic catalysis of N vacancies and similar to 5 nm Au nanoparticles promoted the highly sensitive electrochemical determination of lead(ii) using an Au/N-deficient-C3N4 nanocomposite. Environ-Sci Nano. 2019;6(6):1895–908. https://doi.org/10.1039/c9en00114j.
49. Xu RX, Yu XY, Gao C, Liu JH, Compton RG, Huang XJ. Enhancing selectivity in stripping voltammetry by different adsorption behaviors: the use of nanostructured Mg-Al-layered double hydroxides to detect Cd(II). Analyst. 2013;138(6):1812–8. https://doi.org/10.1039/c3an36271j.
50. Tibbetts DF, Davis J, Compton RG. Sonoelectroanalytical detection of lead at a bare copper electrode. Fresenius J Anal Chem. 2000;368(4):412–4.

Publisher's note Springer Nature remains neutral with regard to jurisdictional claims in published maps and institutional affiliations.